Progress In Electromagnetics Research, Vol. 152, 1–15, 2015

Can Maxwell's Fish Eye Lens Really Give Perfect Imaging? Part III. A Careful Reconsideration of the "Evidence for Subwavelength Imaging with Positive Refraction"

Sailing He[1, 2, *], Fei Sun[1, 2], Shuwei Guo[1], Shuomin Zhong[1], Lu Lan[1], Wei Jiang[1], Yungui Ma[1], and Tiantain Wu[1]

Abstract—Many scientists do not believe that Maxwell's fish eye mirror (MFEM) can provide perfect imaging even if there is a drain array around the imaging points. However, one microwave experiment found a case where a 0.2λ resolution could be achieved in an MFEM experiment [1]. In this paper, we show that the MFEM cannot resolve two imaging points at such a subwavelength resolution in most cases even in the presence of a drain array, and an extraordinary case of subwavelength imaging requires a particular phase difference between two coherent sources. Both numerical simulations and experimental results show that the phase difference of two subwavelength-distanced coherent sources greatly influences the field distribution around the drain array. In very few cases (when the phase difference of the two sources is chosen to be a very specific value), we might resolve the image points in the drain array under the assumption that the power absorbed by the scanning cable on the left side of the drain array should be symmetric to that on the right side of the drain array [1]. However, in most cases, we cannot obtain a super-resolution imaging, as other drains around the image points will greatly influence the imaging. We also note that the experiment assumed that the power absorbed by the scanning cable on the left and the right sides of the drain array is symmetric is not correct for the experiment reported in [1], as the drain array itself is not symmetric. The highly non-symmetric distribution of the absorbed power is also verified by our simulation and experimental results. The experimental "result" of resolving two image peaks could potentially be recovered using only a single image peak, which demonstrates the wrong assumption of mirror symmetry. Comparisons and comments on perfect passive drains, "super-resolution" in a spherical geodesic waveguide, and time reverse imaging are also given.

1. INTRODUCTION

The purpose of this paper is to clarify the so-called experimental "evidence" for subwavelength imaging with positive refraction [1] (see also [2]). We have made several attempts to extend this work and come to the unfortunate realization that the so-called "super resolution" requires a specific phase difference between the two coherent source rods and the original report relied on an incorrect assumption regarding the symmetry of the signal on the left and right coaxial cables.

In 2009, Leonhardt proposed that perfect imaging can be achieved without a negative refraction index [3]. Leonhardt claimed that Maxwell's fish eye lens (MFEL), which can provide ideal imaging from the perspective of geometric optics, can also provide perfect imaging from the perspective of wave optics (i.e., the resolution can be infinite theoretically). He also proposed that a 2D Maxwell's fish eye

Received 1 May 2015, Accepted 1 June 2015, Scheduled 2 June 2015

* Corresponding author: Sailing He (sailing@jorcep.org).

[1] Centre for Optical and Electromagnetic Research, Zhejiang Provincial Key Laboratory for Sensing Technologies, JORCEP, East Building #5, Zijingang Campus, Zhejiang University, Hangzhou 310058, China. [2] Department of Electromagnetic Engineering, School of Electrical Engineering, Royal Institute of Technology (KTH), Stockholm S-100 44, Sweden.

mirror (i.e., a Maxwell's fish eye lens enclosed by a mirror) could theoretically provide perfect imaging, which has been an intense subject of controversy [4–17]. Blaikie commented that the super-resolution is due to the active drain at the image point but not the property of the lens [4], and hence many other types of imaging system can also achieve such subwavelength focusing with the help of a drain, e.g., we can obtain a sub-wavelength focused spot at the image point if there is only one drain exactly located at the image point in any absolute image system (such as a mirror-enclosed elliptical cavity filled with air when a line current is at one focus and a drain is exactly located at the other focus [5]). Blaikie used the finite element method (FEM) to simulate a case when only a line current source exists in the MFEM without any active drain at the image point and did not find any super-resolution image [4]. Leonhardt replied to Blaikie's comment that only one source in the MFEM without any drains is 'in conflict with causality and hence unphysical' [6]. Later Kinsler and Favaro gave a comment on Leonhardt's argument of causality, and used a finite difference time domain (FDTD) simulation to show that causal solutions can be obtained even without any active drains in an MFEM [7]. As the reply to Kinsler's comment, Leonhardt claimed that a pulse in time domain can be perfectly focused [8]. However, recent study shows that an MFEL with an optimal active drain still cannot give a perfect image for a pulse in time domain (as the drain also absorbs energy even if the drain is not at the image point) [9]. In our previous parts (Part I and Part II) of the study on this subject, we have obtained two important results: firstly, MFEM cannot give a super-resolution imaging without the drain due to the high order modes (i.e., evanescent waves) cannot reach the image position to restore the fine details of the object [10]; Secondly, MFEM still cannot give a super-resolution imaging even if some passive coaxial cable drains are used due to the fact that the passive drains located not exactly at the image point still absorb energy and influence the field intensity in the whole structure [11]. In 2010, Leonhardt extended his idea to the 3D case, and proposed that an impedance-matched 3D MFEL (i.e., $\varepsilon = \mu = n$) could still give a perfect image even for the lossy medium case [12]. Merlin gave a comment on Leonhardt's 3D theory and showed the unlimited resolution was due to the drain artificially set exactly at the image point [13].

Whether an MFEL/MFEM can give a perfect imaging causes a hot debate in recent years [16]. The subwavelength focusing is due to the drain in MFEL/MFEM but not the medium itself [4, 5, 10]; if there are some additional passive drains around the imaging point, they will greatly influence the imaging effect (e.g., we may also get a focused spot at other drains that are not located at the image point) and an MFEM cannot give a super-resolution imaging if there are some other drains around the imaging points [9, 11, 17].

In 2011, it was shown in a microwave experiment that an MFEM can resolve two imaging points even if there are some additional drains around the image points, obtaining a resolution of 0.2λ [1, 2]. In [1, 2], Leonhardt presented this as an evidence of super-resolution imaging in the microwave MFEM. In this paper, we present a more objective interpretation of this experimental result of subwavelength imaging as due to a source coherence and mirror symmetry assumption.

2. MODEL OF DRAINS IN AN MFEL/MFEM

In this section we briefly review some analytical formula in an MFEL/MFEM. The refraction index of an MFEL/MFEM can be written as [3]:

$$n = \frac{2}{1 + (r/a)^2}. \tag{1}$$

The MFEL is filled in the whole 2D plane. The MFEM is enclosed by a PEC circle with radius a. $r^2 = x^2 + y^2$ is the coordinate variable in the cylindrical coordinate system. The relations between locations of the object and image in an MFEL/MFEM can be determined from the stereographic projection [3]:

$$z_i = \begin{cases} -\dfrac{1}{z_o^*}, & \text{in an MFEL} \\ -z_o, & \text{in a MFEM} \end{cases}, \tag{2}$$

where $*$ means the complex conjugate, and z_o and z_i are complex coordinate of the source and image (e.g., $z = x + iy$), respectively. The complex amplitude of monochromatic electric field $E(x, y)e^{-i\omega t}$ for

the TE wave satisfies the Helmholtz equation in the region without sources and drains:

$$\Delta E + n^2 k_0^2 E = 0. \tag{3}$$

The field distribution in an MFEL/MFEM with one line current source at $z = z_o$ (without any drain) can be given as:

$$E_s = \begin{cases} \dfrac{1}{4\sin(v\pi)} P_v\left(\xi\left(w\left(z\right)\right)\right), & \text{in an MFEL} \\ \dfrac{1}{4\sin(v\pi)}\left[P_v\left(\xi\left(w\left(z\right)\right)\right) - P_v\left(\xi\left(w\left(\dfrac{1}{z*}\right)\right)\right)\right], & \text{in an MFEM} \end{cases}. \tag{4}$$

The field distribution in an MFEL/MFEM with one line current source at $z = z_o$ and one perfect drain at $z = z_i$ can be given as:

$$E = \begin{cases} \dfrac{1}{4\sin(v\pi)}\left\{P_v(\xi(w(z))) - e^{iv\pi} P_v(-\xi(w(z)))\right\}, & \text{in an MFEL} \\ \dfrac{1}{4\sin(v\pi)}\left\{\left[P_v(\xi(w(z))) - P_v\left(\xi\left(w\left(\dfrac{1}{z*}\right)\right)\right)\right] - e^{iv\pi}\left[P_v(-\xi(w(z))) - P_v\left(-\xi\left(w\left(\dfrac{1}{z*}\right)\right)\right)\right]\right\}, & \text{in an MFEM} \end{cases} \tag{5}$$

where $v = (\sqrt{4k_0^2 + 1} - 1)/2$, $\xi = (|w|^2 - 1)/(|w|^2 + 1)$ and $w = (z - z_o)/(zz_o^* + 1)$. $P_v(\xi)$ and $Q_v(\xi)$ are the Legendre functions of the first kind and the second kind, respectively. The field distributions with/without a perfect drain in an MFEM are shown in Figure 1. Note that the amplitude of the line current is $1/(i\omega\mu_0)$ in Equations (4) and (5), which corresponds to a unit delta source on the right side of the Helmholtz Equation (3) [3, 19].

Leonhardt only gave the analytical solution for one source and one perfect drain exactly at the image point [3]. However, no analytical solutions are given for the case when the drain is not exactly at the image point (only some simulation study for this case). Here we will give the analytical solutions for the case with many line currents sources and multiple drains. If we only set a line current source at the MFEM/MFEL without introducing any drains, it can only excite the source mode (see Eq. (4) and Figure 1(b)), and thus there is no extremely sharp field peak around the image point. If we set a perfect drain at the image point of the line current source, we can find an extremely sharp field peak around the image point (Eq. (5) and Figure 1(a)). According to the superposition principle in

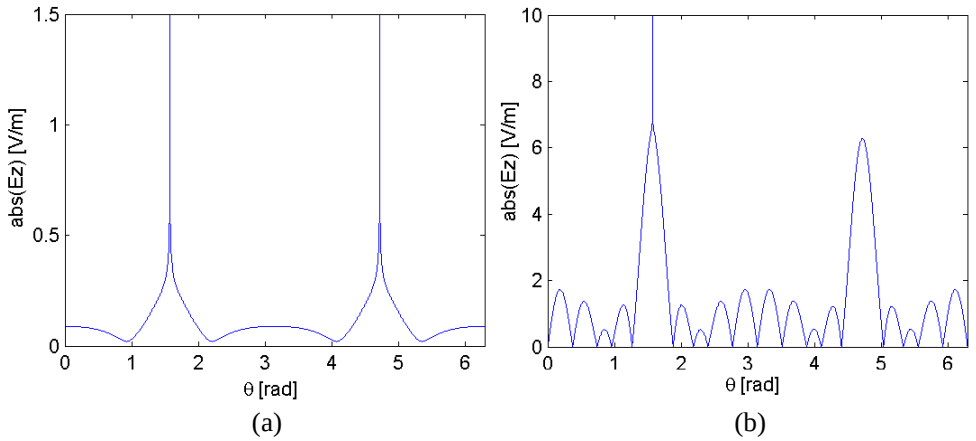

Figure 1. The absolute value of the electric field distribution in a 2D MFEM with $a = 5\,\text{cm}$ when we set a line current source at $(0, -0.6a)$ with wavelength $\lambda_0 = 3\,\text{cm}$ for the TE polarization. (a) We also set a perfect drain at the image point $(0, 0.6a)$. The field distribution along the radius $r = 0.6a$ can be calculated by Eq. (5). (b) No drains are set at the image point. The field distribution along the radius $r = 0.6a$ can be determined by Eq. (4).

electromagnetic theory (as the Helmholtz Eq. (3) is a linear equation), we can deduce that a perfect drain's mode in an MFEM/MFEL will be generated, if we put a perfect drain in an MFEM/MFEL. From Eq. (5) subtracted Eq. (4), this perfect drain's mode can be written as:

$$E_d = \begin{cases} \dfrac{-e^{iv\pi} P_v\left(-\xi\left(w\left(z\right)\right)\right)}{4\sin\left(v\pi\right)}, & \text{in an MFEL} \\ \dfrac{-e^{iv\pi}}{4\sin\left(v\pi\right)}\left[P_v\left(-\xi\left(w\left(z\right)\right)\right) - P_v\left(-\xi\left(w\left(\dfrac{1}{z*}\right)\right)\right)\right], & \text{in an MFEM} \end{cases}. \tag{6}$$

If no drains are introduced, there is no drain's modes in an MFEM/MFEL, and thus a line current source can only excite the source mode and no extremely sharp field around its image. If we set a perfect drain at the image point, a drain's mode will be generated, and then a line current source will not only excite the source mode (Eq. (4)) but also the drain mode (Eq. (6)). According to the superposition principle, the total field distribution is the sum of the source mode and the drain mode (Eq. (5)), and thus an extremely sharp field will appear around both the source and drain. Thus if a perfect drain is set exactly at the image point, when this drain's mode is excited, there will be an extremely sharp field around the drain. The observer will see a "perfect image" at the drain point. However, if we set a line current source and a perfect drain no longer at the image point (we can still use Eq. (6) to calculate the drain's mode), both the source's mode and drain's mode will still be excited. However, this time we will see two extremely sharp field peaks around the source point and the drain point (not located at the image point), while no such extremely sharp field peak would appear at the image point. This is not an imaging process but a process of mode excitation and superposition: if we cannot set the perfect drains at exactly the image points, we will never obtain perfect imaging of the sources.

Furthermore, if we set one line current source and many perfect point-like drains at the MFEM/MFEL, many perfect drain's modes will be excited. Even if some perfect drain's modes are slightly excited, they will seriously affect the field distribution in the MFL (Maxwell's fisheye lens) mirror due to the fact that the field around the perfect drain in Leonhardt's analytical model is infinitely sharp (i.e., the field at the perfect drain point is infinitely large). This can be easily seen in Figure 2, when we set a line current source at $(0,\ -0.6a)$ and two or three perfect passive drains in the same circle of the source. If perfect drains are passive, the total field in MFL mirror can be written approximately as:

$$E_{total} = \sum_{m=1}^{M} E_s^{(m)} + \sum_{n=1}^{N} \alpha_n E_d^{(n)}. \tag{7}$$

E_s means the source mode which can be calculated by Eq. (4), and M is the total number of the sources. E_d is the perfect drain mode which can be determined by Eq. (6) and N is the total number of the passive drains. Factor α_n indicates the excitation degree of the n-th passive perfect drain (by all the sources) and it can be determined by the relative amplitude of electric field at the n-th drain point when no drains are set in the MFL mirror. If the perfect drain is active, the total field in MFL mirror can be written as:

$$E_{total} = \sum_{m=1}^{M} E_s^{(m)} + \sum_{n=1}^{N} E_d^{(n)}. \tag{8}$$

No matter the perfect point-like drain is passive or active, any additional perfect point-like drains will give a serious adverse effect to the image (see Figures 2 and 3). In practical imaging, we do not know the locations of image points in advance. We have to set many passive drains around the images, thus many modes corresponding to these drains will be excited in this MFEM. The above results have shown that these perfect drains will affect the whole field distribution in an MFEM which leads to some extremely sharp peaks no longer correspond to the distributed images, but merely as a result of the superposition of the modes corresponding to these perfect drains.

The key of Leonhardt's method to achieve a perfect focusing in an MFEL or MFEM is introducing a perfect drain that can absorb the incoming wave without any scattering. There are some studies on how to achieve such a drain in practice [9, 18–20]. The drain can be either active (e.g., a dipole [9]) or passive (e.g., some lossy medium or a coaxial cable [1, 18–20]). Coaxial cables have been utilized to mimic the drain in Leonhardt's analytical model inside an MFEM [1]. However, coaxial cables cannot

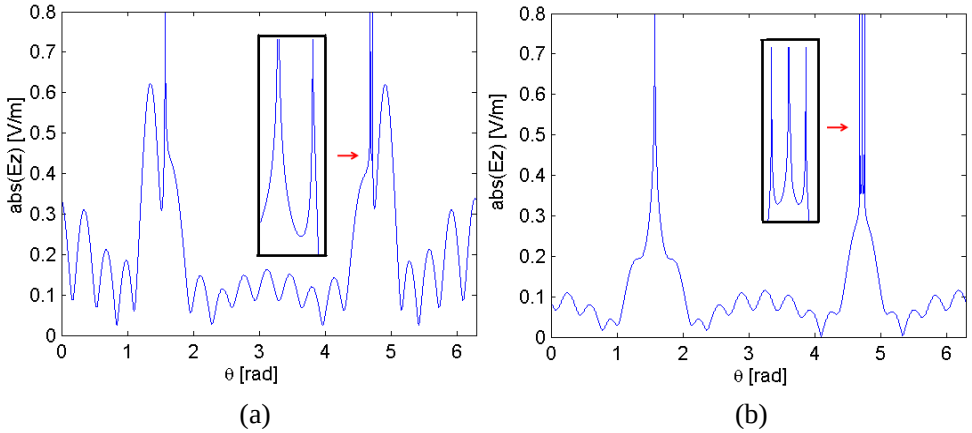

Figure 2. The absolute value of the electric field distribution in a 2D MFEM with $a = 5\,\text{cm}$ in the presence of *passive* drains. We set one line current source at $(0, -0.6a)$ with wavelength $\lambda_0 = 3\,\text{cm}$ for TE polarization. (a) The field distribution along the radius $r = 0.6a$ when two passive perfect drains are set at $(0,\ 0.6a)$ and $(-0.6\sin(0.034)a,\ 0.6\cos(0.034)a)$ (0.05λ apart in the same circle of $r = 0.6a$). The field distribution can be calculated by Eq. (7) with $\alpha_1 = 0.5047$ and $\alpha_2 = 0.4953$. (b) The field distribution along the radius $r = 0.6a$ when three passive perfect drains are set at $(0,\ 0.6a)$, $(-0.6\sin(0.034)a,\ 0.6\cos(0.034)a)$ and $(0.6\sin(0.034)a,\ 0.6\cos(0.034)a)$. This means that three passive drains are 0.05λ apart from its neighbor in the same circle of $r = 0.6a$. The field distribution can be calculated by Eq. (7) with $\alpha_1 = 0.3376$, $\alpha_2 = 0.3314$ and $\alpha_3 = 0.331$.

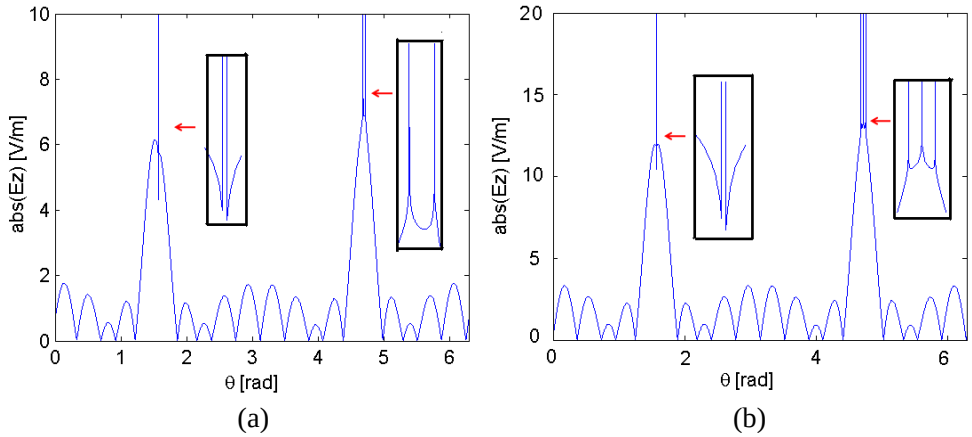

Figure 3. The absolute value of the electric field distribution in a 2D MFEM with $a = 5\,\text{cm}$ in the presence of *active* drains. We set a line current source at $(0, -0.6a)$ with wavelength $\lambda_0 = 3\,\text{cm}$ for TE polarization. (a) The field distribution along the radius $r = 0.6a$ when two active drains are set at $(0,\ 0.6a)$ and $(-0.6\sin(0.034)a,\ 0.6\cos(0.034)a)$ (0.05λ apart in the same circle of $r = 0.6a$). The field distribution can be calculated by Eq. (8). (b) The field distribution along the radius $r = 0.6a$ when three active drains are set at $(0,\ 0.6a)$, $(-0.6\sin(0.034)a,\ 0.6\cos(0.034)a)$ and $(0.6\sin(0.034)a,\ 0.6\cos(0.034)a)$. This means that three passive drains are 0.05λ apart from its neighbor in the same circle of $r = 0.6a$. The field distribution can also be calculated by Eq. (8).

behave exactly as a perfect drain in Leonhardt's theoretical model due to the following reasons: Firstly, the size of the drain should be infinitely small (e.g., a point-like drain) in Leonhardt's theoretical model. A coaxial cable has a finite cross section which limits the resolution. Secondly, the drain in Leonhardt's theoretical model will not produce any scattering to the converging wave. For a coaxial cable, it produces some scattering even if terminated by some impedance matched absorber (due to the mode mismatch between the mode in a coaxial cable and the mode in an MFEM).

A perfect passive drain (PPD) has been designed with some lossy inhomogeneous medium [19], which agrees very well with Leonhardt's theoretical model. It means that such a PPD does not produce any additional scattering if it is located at the right position and behaves exactly like a point-like perfect drain in Leonhardt's theoretical model when the radius of the PPD approaches zero. There are still no studies on whether MFEL can give a perfect imaging if a PPD is not exactly located at the image point or if a drain array is introduced. Previous studies on whether an MFEL or MFEM can give a good image when a drain array is introduced are for the cases that drains are approximated by coaxial cables but not PPDs. Here we show that an MFEL still cannot give a super-resolution imaging even if a PPD is used.

A PPD is a circular lossy inhomogeneous non-magnetic medium with radius R, which fully absorbs the power of incoming wave without producing any scattering wave if it is located exactly at the image point [19]. The point-like PPD can be obtained by taking limitation $R \to 0$.

Before performing some numerical simulation, we can summarize the whole process of designing a PPD in three steps: First, we should choose the working wavelength λ_0 and the location of the object point (the location of image point is fixed according to Eq. (2)). If the source is located at (x_0, y_0), its image will appear at $(-x_0/(x_0^2+y_0^2), -y_0/(x_0^2+y_0^2))$. Second, we need to choose the size R of the PPD,

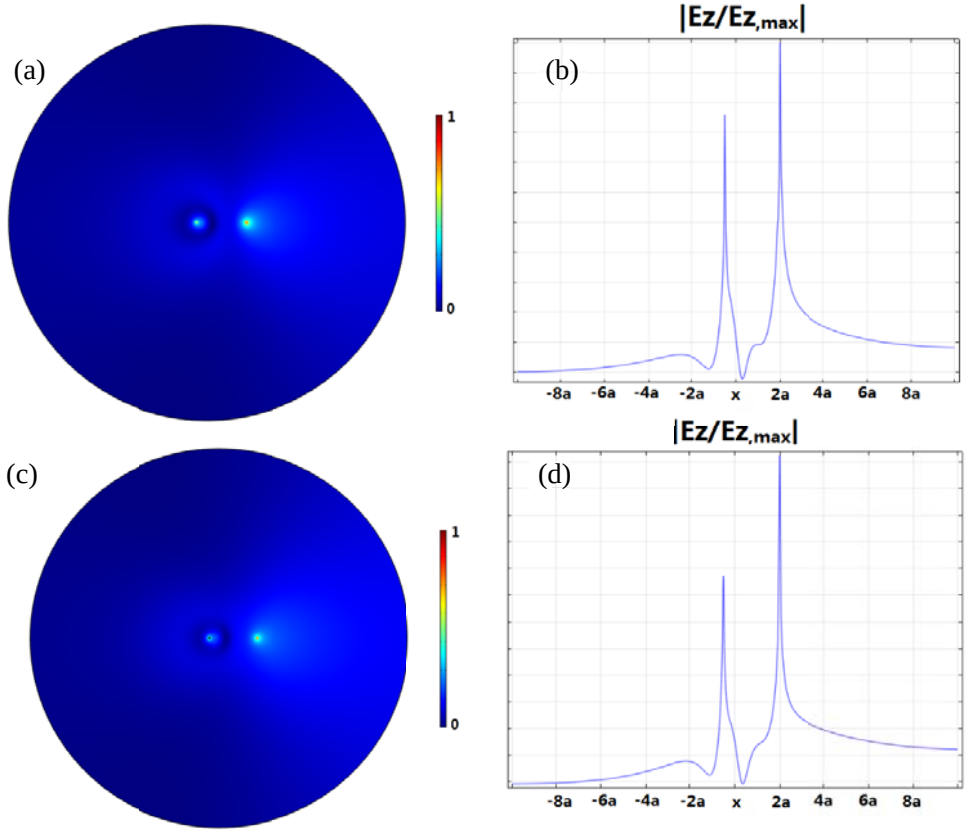

Figure 4. The normalized absolute value of electric field distribution in a 2D MFEL for TE wave with working frequency $f = 10\,\mathrm{GHz}$ and radius $a = 0.01\,[\mathrm{m}]$. (a) and (b) a line current is located at the object point $(2a, 0)$ and a perfect active point drain is exactly at the image point $(-0.5a, 0)$ which exactly agrees with Leonhardt's analytical model. (c) and (d) a line current is located at the object point $(2a, 0)$ and a PPD with $\xi_d = 0.999$, $R = 0.028a$, and $\varepsilon_d = 64.2689 + 36.693i$ is located at a slightly deviated position $(x_c = -0.5003a,\ y_c = 0)$. (a) and (c) are field distributions in the whole 2D MFEL. (b) and (d) are normalized field distributions along the x direction. Note that the field amplitudes are not infinitely large (but quite large) at the source and the drain because numerical FEM simulation with a finite mesh size can not give an infinitely large field value at any grid point.

and the center $(x_c,\, y_c)$ of the circular PPD, which can be determined by [19]:

$$R = \frac{\sqrt{1-\xi_d^2}\left(1+x_0^2+y_0^2\right)}{\left(1+x_0^2+y_0^2\right)\xi_d + \left(x_0^2+y_0^2\right) - 1} \tag{9}$$

$$\begin{cases} x_c = -\dfrac{2x_0}{\left(1+x_0^2+y_0^2\right)\xi_d + \left(x_0^2+y_0^2\right) - 1} \\ y_c = -\dfrac{2y_0}{\left(1+x_0^2+y_0^2\right)\xi_d + \left(x_0^2+y_0^2\right) - 1} \end{cases} \tag{10}$$

Note that parameter ξ_d should be chosen in advance, which determines the size of the PPD: as $\xi_d \to 1$, the size of the PPD approaches to a point (i.e., a point-like PPD), and the model gets closer to Leonhardt's analytical model. Finally, we need to determine the lossy medium inside the PPD [19]:

$$n_d = \frac{2\sqrt{\varepsilon_d}}{1+r^2}, \tag{11}$$

where ε_d is a complex number which can be calculated by

$$\varepsilon_d = \frac{v'(v'+1)}{\omega^2\mu_0\varepsilon_0}. \tag{12}$$

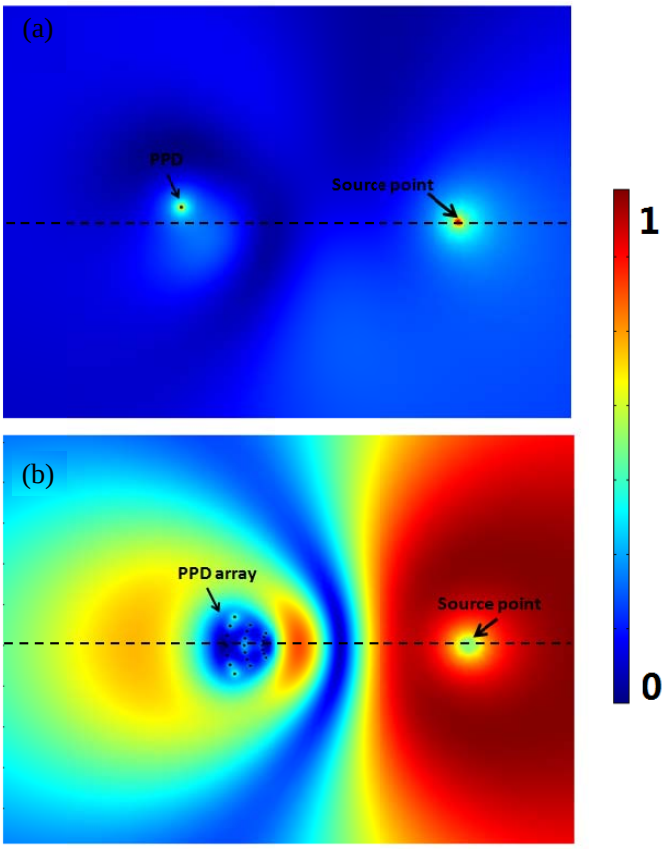

Figure 5. FEM simulation results: we plot the normalized absolute value of electric field's z component for the TE wave case ($f = 10\,\text{GHz}$ and $a = 0.01$ [m]). A line current is set at $(2a,\, 0)$ as the object point. (a) The PPD is not at the image point $(-0.5a,\, 0)$ but at the position 15 [deg] rotated (around the origin $(0,\, 0)$) from the image point. (b) A PPD array is set around the image point. The dashed line indicates the x axis, on which the image point is located.

Here v' can be determined by solving the following equation:

$$\frac{\frac{dP_{v'}|_{\xi_d}}{d\xi}}{P_{v'}(\xi_d)} = \frac{\frac{dP_v|_{\xi_d}}{d\xi} + i\frac{2}{\pi}\frac{dQ_v|_{\xi_d}}{d\xi}}{P_v(\xi_d) + i\frac{2}{\pi}Q_v(\xi_d)} \tag{13}$$

Previous studies have verified that the field distribution outside such a PPD can be used to mimic Leonhardt's analytical model [19]. We use numerical simulation based on the finite element method (FEM) to verify the performance of such a PPD (see Figure 4). The field distribution in a 2D MFEL for the case of an active drain in Leonhardt's analytical model (see Figures 4(a) and (b)) and that for the case of a PPD (see Figures 4(c) and (d)) located exactly at the image point are almost the same, which shows that we can use a PPD to mimic the drain in Leonhardt's analytical model. The simulated results agree with the theoretical prediction very well: as $\xi_d \to 1$, the size of a PPD approaches to a point, and the field distribution outside the PPD gets closer to the perfect point-like drain in the analytical model. The previous study does not consider the case that a PPD is not exactly located at the image point. We use FEM simulation to study the case when a PPD is slightly displaced from the image point (Figure 5(a)), and the results show that such a PPD still absorbs energy and causes a field intensity peak (not at the image point) even if it is displaced from the image point. Figure 5(b) shows that field intensity peaks also appear at non-image positions when a PPD array is put around the image point. Both Figures 5(a) and (b) demonstrate that an MFEL cannot give a super-resolution imaging even if the perfect passive drains are introduced.

3. NUMERICAL SIMULATION

We use the FEM to simulate the microwave experiment reported in [1]. The numerical simulation is conducted by the commercial software COMSOL Multiphysics. The structure we simulate here is almost the same as the one used in the microwave experiment reported in [1], and the only difference is that the outer radius of the coaxial cables is a bit smaller than the practical size (because in simulation we cannot create the geometric modeling of the coaxial cables if we set them very close to each other while keeping the original size of the radius).

The structure we simulate here is shown in Figure 6(a), where the two sources are identical coaxial cables separated by 0.2λ on the same circle $r = 0.6a$ with $a = 5\,\text{cm}$ (the local wavelength $\lambda = \lambda_0/n$; $\lambda_0 = 3\,\text{cm}$). Ten passive drains (also coaxial cables) are separated by 0.05λ on the same circle $r = 0.6a$ and terminated by a perfectly matched layer to mimic an impedance match condition. Note that among the 10 drains there are two drains that are located exactly at the two image points. The MFEM is inserted in two parallel perfect electric conductors (PECs) with a distance of 5 mm. Sources and drains are inserted into the MFEM 4.5 mm and 2 mm from the bottom PEC, respectively. All coaxial cables in simulations have a core diameter of 0.5 mm and an outer diameter of 1 mm (Teflon isolator with relative electric permittivity 2.55 is filled between the two PEC boundaries). As shown in Figures 6(b)–(f), the field distribution around the drain array changes if the phase difference between the two sources changes. This means that the phase difference will greatly influence the field distribution around the drain array. Three years ago, the first author of the present paper started to suspect that the microwave experiment reported in [1] is just a special case when the interference field is maximized around the two drains located at the image points when the phase difference between the two coherent sources has a specific value. It took nearly 3 years to complete our experiment and clarify the conclusions reported in [1]. In most cases, the maximum interference field is not exactly at a drain located at the image point but is at some other drains around the image point.

In the microwave experiment reported in Ref. [1], a scanning coaxial cable is inserted 2 mm into the MFEM from the top PEC plate. Compared with the case without the scanning cable (e.g., Figure 6), the scanning cable will influence the field distribution in the MFEM. We also use the FEM to simulate this case (see Figure 7). According to the simulation results, the phase difference of the two sources will greatly influence the power absorbed by the scanning cable. The power intensity (roughly proportional to the power absorbed by the scanning probe as a detector) at the central cable between the two image points could be smaller (e.g., when the phase difference is 80°) or larger (e.g., when the phase

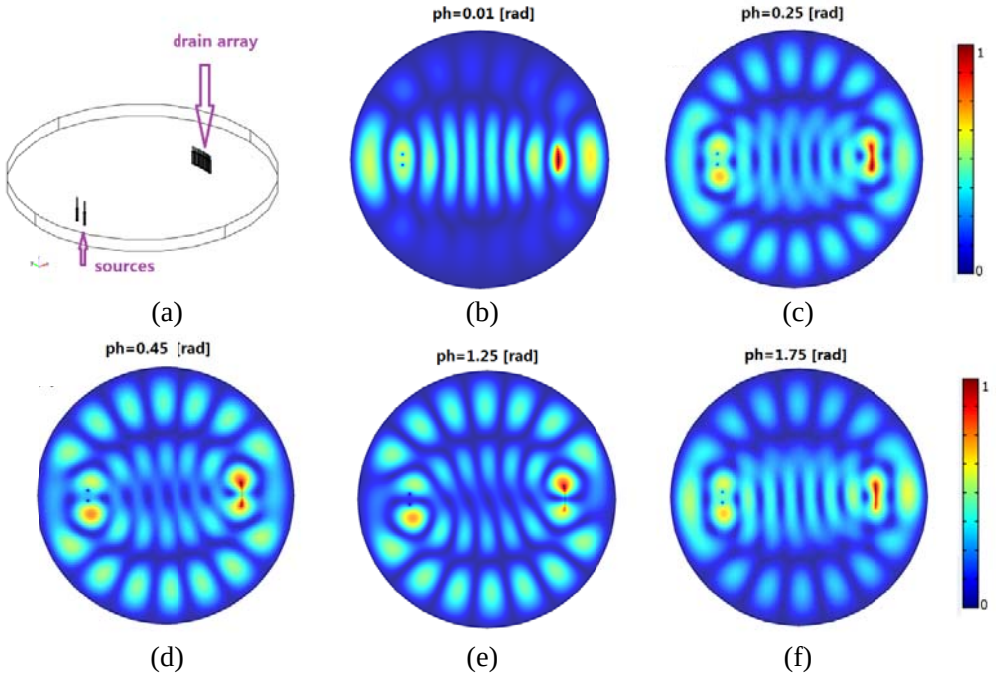

Figure 6. (a) The structure of a 2D MFEM without the scanning cable. The drain array consists of 10 coaxial cables separated by 0.05λ. (b)–(f) FEM simulation results: the normalized absolute value of the z-component of the electric field 3 mm above the bottom PEC plate when the phase difference (ph) of the two sources changes from 0.01 rad to 1.75 rad. We keep the amplitude of the two sources the same when changing the phase difference. Note that we do not introduce any scanning cable (inserted from the top PEC plate) in this simulation.

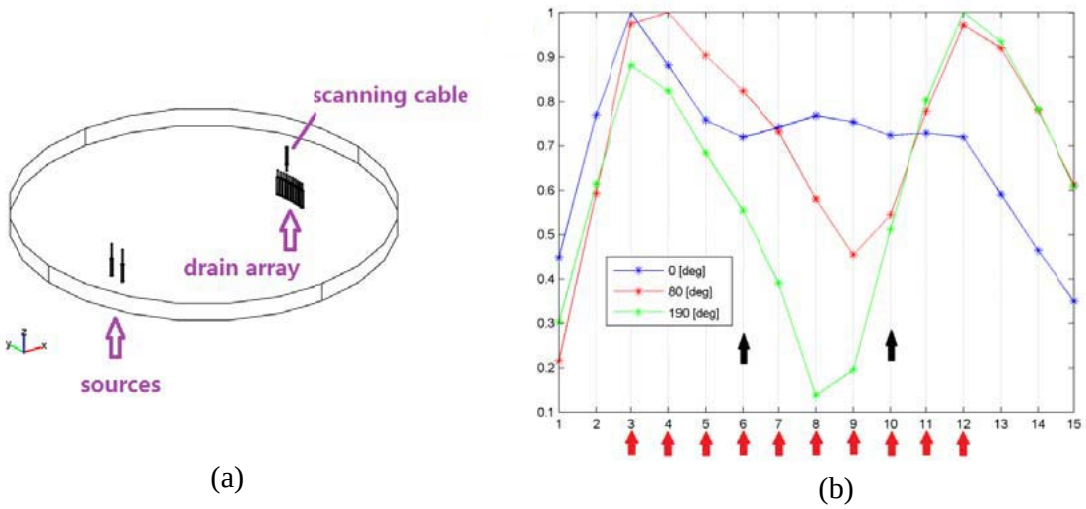

Figure 7. (a) The structure of a 2D MFEM with the scanning cable. The scanning cable is inserted into the structure from the top PEC, and scans the circle $r = 0.6a$ around the drain array (10 coaxial cables separated by 0.05λ). The scanning step is 0.05λ. (b) FEM simulation results for the structure of a 2D MFEM with the scanning cable. We plot the normalized power absorbed by the scanning cable (as the detector). The two black arrows indicate the location of the two drains that are exactly at the image points. Ten passive coaxial cables are located at x-axis points from labels 3 to 12, indicated by small red arrows.

Table 1. The parameters in each discrete layer of our MFEM. From the center to outer layer, we label these layers with numbers 1 to 20. The different colors indicate different powders filled in the layers.

The number of the layer	Effective refraction index	Relative permitvity of the powder	The number of units
1	1.998750781	4	
2	1.988812927	4	
3	1.969230769	2.5	16
4	1.940570042	2.5	22
5	1.903628792	2.5	28
6	1.859384079	2.5	35
7	1.8089316	2.5	41
8	1.753424658	2.5	47
9	1.694017999	2.5	53
10	1.6318205	2.5	60
11	1.567858893	1	66
12	1.503053077	1	72
13	1.438202247	1	79
14	1.373980249	1	85
15	1.31093814	1	91
16	1.249511909	1	97
17	1.19003347	1	104
18	1.132743363	1	110
19	1.077803974	1	116
20	1	1	0

difference is 0°) than the power intensity at the cables located at the image points (i.e., the situation changes with the phase difference). However, the simulation model cannot be completely equivalent to the experimental model due to the following reasons. Firstly, each coaxial cable in the experiment is terminated by an impedance-matched absorber. In simulation we can use a model of the matched absorption boundary condition or perfect match layer (PML) to mimic this. Secondly, each coaxial cable in the experiment can be bent and stretched vertically or compressed horizontally (to reduce the outer diameter of a coaxial cable), and hence the distance between any two neighboring coaxial cables (used as passive drains) can be 0.05λ even the outer diameter of each coaxial cable is 2.1 mm (the cables used in [1] have an outer diameter of 2.1 mm, with a 1.68 mm teflon isolator and 0.5 mm inner conductor). However, we have to slightly reduce the outer diameter of each coaxial cable (to 1 mm) in simulation to ensure that the distance between any two neighboring coaxial cables (used as passive drains) can remain at 0.05λ. From three simulation curves in Figure 7(b) one sees clearly that the power absorbed by the scanning cable is always highly non-symmetrical around the midpoint (i.e., around the central drain located at position 8) of the two image positions. This is due to the fact that there are five passive drains on the left-hand side of the central drain (at position 8) and only four passive drains on the right-hand side of the central drain. For some phase difference there appears only one peak, and for some other phase difference there may appear two non-symmetrical peaks (but not at the two image points). We also designed an experiment to verify our idea inspired by our simulation results in this section.

4. EXPERIMENTAL RESULTS

We made an MFEM that is exactly the same as the one used in the reported microwave experiment [1]. The sample is shown in Figure 8(a). We divide the whole MFEM equally into 20 discrete layers. The effective refraction index of each layer is given in Table 1. The experimental setup and measured results for the case with a scanning cable are given in Figures 8(b) and (c), respectively. We should note that like the experiment reported in [1], the source signal from a single vector network analyzer is divided (through a power divider) into two parts that are connected to the two sources in the MFEM, and hence the two sources are coherent in the experiment.

As we can see from Figure 8(c), the phase difference between the two sources greatly influences the relative amplitude of the electric field around the drain array. We cannot gradually change the phase difference of the two sources in the experiment (the phase shifter requires manual adjustment, and continuous adjustment is difficult). We only provide some values of the phase difference that we can obtain in the experiment, and none of these cases show any super-resolution imaging ability of the MFEM. Similar to our previous numerical simulation result (Figure 7(b)), our experimental results (Figure 8(c)) show clearly that the power absorbed by the scanning cable is always highly non-symmetrical around the central cable (located at position 8). This non-symmetry of the power absorbed by the scanning cable is due to the fact that there are five passive coaxial cables on the left side of the central cable and only four passive cables on the right side of the central cable (ten coaxial cables in total are used as passive drains, exactly the same as in the experiment reported in [1]).

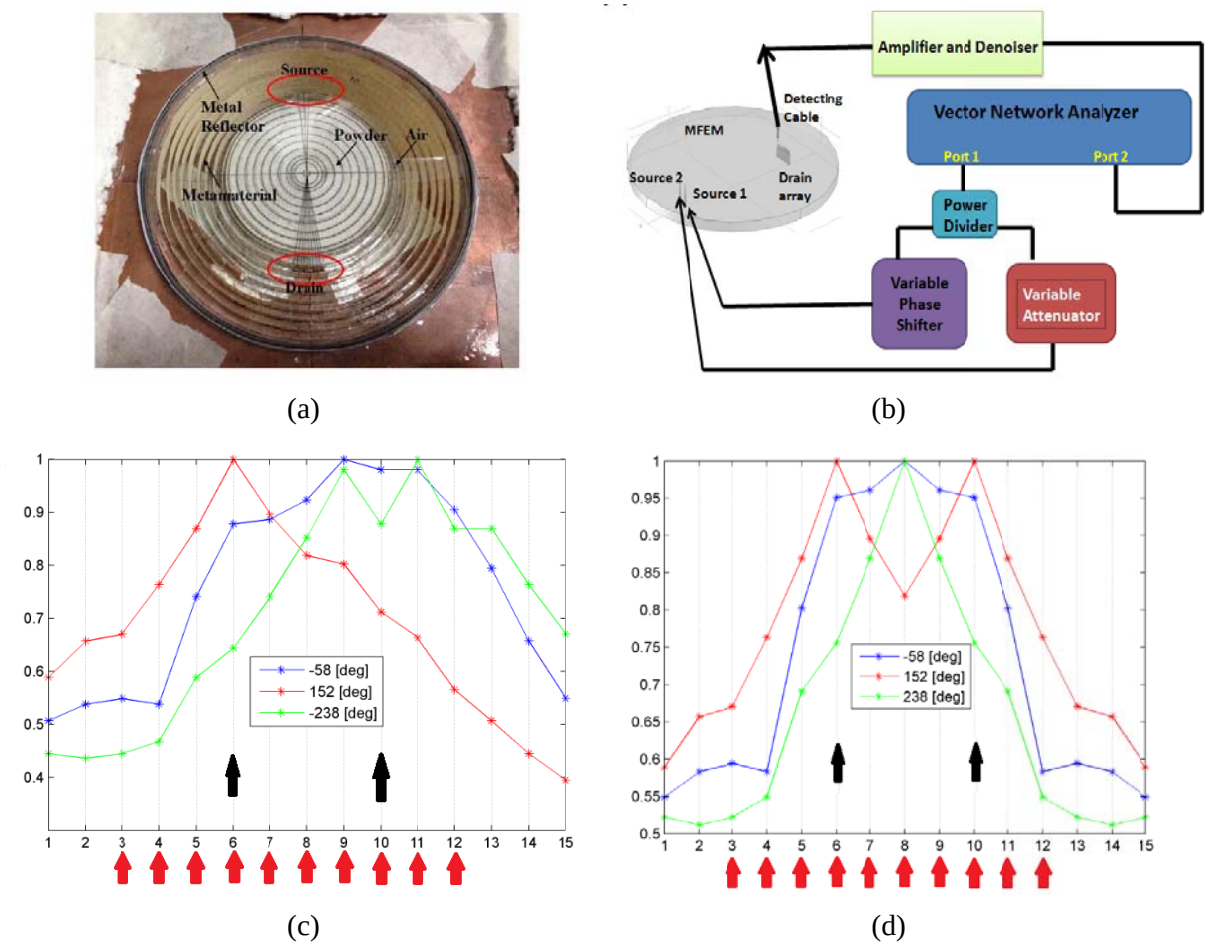

Figure 8. (a) The MFEM used in the experiment. (b) The experimental setup. (c) The normalized measured power absorbed by the scanning cable around the drain array when the phase difference between the two sources changes (while keeping the amplitude of the two sources nearly the same). Different colors indicate different phase difference between the two sources. The black arrows indicate the locations of the two drains that are exactly at the image points. Ten passive coaxial cables are marked at x-axis points from labels 3 to 12, indicated by small red arrows. (d) The normalized measured power absorbed by the scanning cable around the drain array if we measure the power (with the scanning cable) only at the left side of the drain array, and make a plot with a mirror-symmetry assumption (i.e., assuming that the power absorbed by the right side of the drain array is symmetrical to that by the left side).

Two conclusions can be made from our experimental results: the first is that the additional drains around the image will influence the imaging effect of an MFEM, which verifies our previous simulation results [9]. The second is that the phase difference between the two sources will greatly influence the field distribution in the MFEM and particularly the field intensity at each passive coaxial cable, which shows that the coherence of the two sources plays a very important role in this experiment. The experimental results reported in [1] may be an extraordinary case with a very special phase difference between the two sources that happens to resolve two images around the drain array. In the experiment reported in [1], only the left side of the drain array was measured, and the power absorbed by the right side of the drain array was assumed to be symmetrical for this specific lens and measurement setup. Under such an assumption, we can also try to make a plot using only the left part of our measured data in such a mirror-symmetry way (see Figure 8(d)). As we can see when the phase difference between the two sources is about 152° in our experiment, such a plot for the power absorbed by the scanning cable is similar to the one (their Figure 4) given in Ref. [1], as if the two image points in the drain array are resolved. However, for other values of phase difference (e.g., −58°), no high-resolution phenomenon appears even with such a mirror-symmetry assumption. In fact, the assumption that the power absorbed by the scanning cable on the left and the right sides of the drain array should be symmetrical over-simplifies the real situation (actually it is highly non-symmetrical), as the drain array itself is not symmetrical (5 drains are on the left side and 4 drains are on the right side of the center drain), as also verified by both our simulation (Figure 7(b) and our experimental measurement on both sides (see Figure 8(c) without the mirror-symmetry assumption).

5. ABOUT THE 'SUPER-RESOLUTION' IN A SPHERICAL GEODESIC WAVEGUIDE

In 2010, Miñano et al. proposed another device, called the spherical geodesic waveguide (SGW) [21]. The SGW is a spherical waveguide filled with an isotropic medium with refraction index proportional to $1/r$, where r is the distance from the center of the sphere. The spherical waveguide can be realized by two concentric metallic spheres with radius R_M and R_m ($R_M > R_m$). If $R_M - R_m \ll \lambda$, one can ignore the variation of the refraction index and use a constant isotropic medium filled within two spherical shells to realize such an SGW [22, 23]. SGW and MFEL are equivalent imaging systems from the perspective of transformation optics by a stereographic projection (i.e., the TE-polarized electric modes in an MFEL corresponds to the radial-polarized electric modes in an SGW). The relation between the two systems can be summarized as [21]:

$$\begin{cases} E_r = \dfrac{1}{r} E_z \\ H_\theta = \dfrac{1}{r(\cos\theta + 1)} H_\rho \\ H_\phi = \dfrac{1}{r(\cos\theta + 1)} H_\psi \end{cases} \tag{14}$$

Here E_z, H_ρ, and H_ψ are fields for the TE mode in an MFEL with refraction index $n = 2/(1+\rho^2)$; E_r, H_θ, and H_ϕ are fields for the radial-polarized mode (i.e., the electric field contains only the radial component) in an SGW with refraction index $n = 1/r$. Later Miñano's group also claimed that $\lambda/500$ and $\lambda/3000$ super-resolution can be achieved in the SGW for only some discrete frequencies by numerical simulations [22, 23]. In 2014, they claimed their experiment of the SGW could achieve a $\lambda/105$ resolution for a set of specific frequencies and loads [24].

Actually the 'super-resolution' found by Miñano in an SGW is essentially different from the perfect image in an MFEL/MFEM claimed by Leonhardt due to the following reasons:

1) The definition of the super-resolution in an SGW is different from the classic definition in optics. In optics, the super-resolution is often defined as the minimal distance between two object points that we can resolve on the image plane, or the minimal size of the spot that can be obtained on the image plane (without any prior knowledge about the image position) [25]. In an SWG, the super-resolution is defined as 'the minimum displacement of a point receptor that causes a drop of the power to 10% of the value received in the initial position.' [24]. The super-resolution claimed by Miñano's group in

an SGW is just a position sensor with a high sensitivity at some discrete frequencies. Super-resolution is useful mainly for imaging applications (e.g., the detection of some small tumors in breast), in which people do not know the exact locations of the sources of interest (e.g., the locations of the small tumors) and consequently do not know the exact locations (i.e., the image positions of the sources) to put the drains. Therefore, people should put many drains (most of them are not at the image positions) in a possible area if drains should be used in an imaging application, as was done in [1, 2, 9].

2) In Leonhardt's method, a super-resolution can be achieved in an MFEL/MFEM for any frequencies with the drains [3], while the super-resolution is found in an SGW only within a narrow band around discrete frequencies (called notch frequencies) [22].

Therefore, the mechanisms behind two phenomena are different. As we have explained, the super-resolution (according to the classic definition in optics) in Leonhardt's method is due to the drain's effect that can help to produce but not restore the evanescent waves. We can obtain a super-resolution focused spot at the image point if a drain is exactly located at the image point for any frequencies. The 'super-resolution' in an SGW is mainly due to the resonance effect on a spherical surface, similar to the Fabry-Pérot resonance for a plane geometry (we can obtain a sharp transmissivity at some discrete frequencies) [25].

If we set a source at the north pole and a drain (e.g., a coaxial cable) is exactly at the south pole in an SWG, the transmission spectrum has many discrete sharp peaks at the Schumann resonance frequencies [22]. If the drain is slightly shifted from the south pole (e.g., $\lambda/100$), the transmissivity for the frequencies around the Schumann resonance frequencies (referred as the notch frequencies) drops sharply. Miñano's group didn't explain the physical mechanism behind this phenomenon. In 2015, Leonhardt used a 1D model to explain this position-sensitive phenomenon in an SGW [26]. Some standing wave is formed at the notch frequency inside the SGW, and the detector is just located at one of the nodes of the standing wave, and hence the transmission is reduced to zero. False "image" would also appear at the other nodes of the standing wave. The narrow band around the notch frequencies can be used as the highly sensitive position sensor.

We should also note that the 'super-resolution' found in SGW is at near field in their simulation [22, 23] and experiment [24] (i.e., the closest distance between the source and the physical waveguiding structure is less than the wavelength). In near-field, a super-resolution can be easily achieved by some microscope technologies (e.g., using a grating in the near field to make the conversion between the evanescent and propagating waves in a structured illumination microscopy [27], and near-field scanning optical microscope [28]).

6. MFEL VS. TIME REVERSE IMAGING

In an MFEL/MFEM, we need some drains to achieve a subwavelength focused spot, which looks similar to the technique using the time reversal mirror (TRM) with some antennas to obtain a super-resolution [29]. We should note that there are essential differences between the MFEL/MFEM and TRM. TRM can be used for both subwavelength focusing and super-resolution imaging, while MFEL/MFEM can only be used for subwavelength focusing but not for super-resolution imaging even with drains. The reason for this can be explained from the view point of the evanescent waves: In a time reversal imaging process, people can set some randomly distributed subwavelength scatterers (e.g., the antenna array) in the near field of the source, and the evanescent waves are converted to the propagation waves by diffracting off the scatterers [29]. The propagation waves reach the TRM in the far field (they are time-reversed there), and transmit back to the random scatterers. Although the source is removed now, the subwavelength scatterers are still there, which can convert the propagation waves to the evanescent waves. Due to the reciprocity, the propagation waves and the evanescent waves can make a reciprocal conversion, which is the key for super-resolution imaging in a TRM. However in an MFEL/MFEM, the evanescent waves at the image are not restored, but produced by some drains. If the drains are not exactly at the image point, they can still produce evanescent waves and obtain some subwavelength focused spots at the drains, and hence this is not an imaging process but a way to get some subwavelength focusing.

7. CONCLUSIONS AND REMARKS

Both simulation and experimental results in this paper have shown that MFEM cannot provide a perfect image if one introduces some passive drains that are not located at the image points. In the future one might be able to find a rare case that happens to resolve the two image points around the drain array, but this could be merely due to the interference effect of the two coherent sources. The experimental result reported in [1] for subwavelength imaging with positive refraction is not such a very special case to resolve the two image points, but turns a single off-center peak into two peaks through an over-simplified mirror-symmetry assumption. Both our simulation and experimental results have shown clearly that the power absorbed by the scanning cable is always highly non-symmetrical around the central cable in their experimental set-up. In other words, their experimental evidence obtained through mirror-symmetry by no means represents the type of perfect imaging that the paper's discussion claimed.

A perfect imaging not only requires aberration-free stigmatic imaging but also requires an infinite resolution. Evanescent waves play an essential role in super-resolution imaging [30]. In Leonhardt's method, a sharp focused spot is achieved at the image point by adding a drain exactly at the image point, which can help to produce evanescent components. We should note that the evanescent components produced by the drain are not the same as the evanescent components of the original source. At an optical frequency in near field, any metallic tip can produce a sub-wavelength hot point (due to the plasmon property of the metal at an optical frequency), even if they are not outlets of the incident wave.

In this paper we have also made some comparisons and comments on perfect passive drains, "super-resolution" in a spherical geodesic waveguide, and time reverse imaging.

After our thorough efforts to reveal the truth about "evidence for subwavelength imaging with positive refraction", we hope that super-resolution research efforts will be directed to more fruitful avenues in the future.

ACKNOWLEDGMENT

This work is partially supported by the National High Technology Research and Development Program (863 Program) of China (No. 2012AA030402), the National Natural Science Foundation of China (Nos. 61178062 and 60990322), the Program of Zhejiang Leading Team of Science and Technology Innovation, and Swedish VR grant (# 621-2011-4620).

REFERENCES

1. Ma, Y. G., S. Sahebdivan, C. K. Ong, T. Tyc, and U. Leonhardt, "Evidence for subwavelength imaging with positive refraction," *New J. Phys.*, Vol. 13, No. 3, 033016, 2011.
2. Ma, Y. G., C. K. Ong, S. Sahebdivan, T. Tyc, and U. Leonhardt, "Perfect imaging without negative refraction for microwaves," *Physics Optics*, arXiv: 1007.2530, 2010.
3. Leonhardt, U., "Perfect imaging without negative refraction," *New J. Phys.*, Vol. 11, No. 9, 093040, 2009.
4. Blaikie, R. J., "Comment on 'perfect imaging without negative refraction'," *New J. Phys.*, Vol. 12, No. 5, 058001, 2010.
5. Blaikie, R. J., "Perfect imaging without refraction?," *New J. Phys.*, Vol. 13, No. 12, 125006, 2011.
6. Leonhardt, U., "Reply to comment on 'perfect imaging without negative refraction'," *New J. Phys.*, Vol. 12, No. 5, 058002, 2010.
7. Kinsler, P. and A. Favaro, "Comment on 'reply to comment on 'perfect imaging without negative refraction'," *New J. Phys.*, Vol. 13, No. 2, 028001, 2011.
8. Leonhardt, U., "Reply to comment on 'perfect imaging without negative refraction'," *New J. Phys.*, Vol. 13, No. 2, 028002, 2011.
9. Tyc, T. and A. Danner, "Resolution of Maxwell's fisheye with an optimal active drain," *New J. Phys.*, Vol. 16, No. 6, 063001, 2014.
10. Sun, F. and S. He, "Can Maxwell's fish eye lens really give perfect imaging?" *Progress In Electromagnetics Research*, Vol. 108, 307–322, 2010.

11. Sun, F., X. C. Ge, and S. He, "Can Maxwell's fish eye lens really give perfect imaging? Part II. The case with passive drains," *Progress In Electromagnetics Research*, Vol. 110, 313–328, 2010.
12. Leonhardt, U. and T. G. Philbin, "Perfect imaging with positive refraction in three dimensions," *Phys. Rev. A*, Vol. 81, No. 1, 011804, 2010.
13. Merlin, R., "Comment on 'perfect imaging with positive refraction in three dimensions'," *Phys. Rev. A*, Vol. 82, No. 5, 057801, 2010.
14. Leonhardt, U. and T. G. Philbin, "Reply to 'comment on 'perfect imaging with positive refraction in three dimensions"," *Phys. Rev. A*, Vol. 82, No. 5, 057802, 2010.
15. Merlin, R., "Maxwell's fish-eye lens and the mirage of perfect imaging," *J. Opt.*, Vol. 13, No. 2, 024017, 2011.
16. Zhang, X., "Perfect lenses in focus," *Nature*, Vol. 480, No. 7375, 42–43, 2011.
17. Quevedo-Teruel, O., R. C. Mitchell-Thomas, and Y. Hao, "Frequency dependence and passive drains in fish-eye lenses," *Phys. Rev. A*, Vol. 86, No. 5, 053817, 2012.
18. Ma, Y., T. Wu, and C. K. Ong, "Subwavelength drains designed for mirror-closed dielectric lenses," *J. Opt.*, Vol. 15, No. 12, 125705, 2013.
19. González, J. C., P. Benítez, and J. C. Miñano, "Perfect drain for the Maxwell fish eye lens," *New J. Phys.*, Vol. 13, No. 2, 023038, 2011.
20. Xu, L. and H. Chen, "Coherent perfect absorber makes a perfect drain for Maxwell's fish-eye lens," *EPL*, Vol. 100, No. 3, 34001, 2012.
21. Miñano, J. C., P. Benítez, and J. C. González, "Perfect imaging with geodesic waveguides," *New J. Phys.*, Vol. 12, No. 12, 123023, 2010.
22. Miñano, J. C., R. Marqués, J. C. González, P. Benítez, V. Delgado, D. Grabovickic, and M. Freire, "Super-resolution for a point source better than $\lambda/500$ using positive refraction," *New J. Phys.*, Vol. 13, No. 12, 125009, 2011.
23. González, J. C., D. Grabovičkić, P. Benítez, and J. C. Miñano, "Circuital model for the spherical geodesic waveguide perfect drain," *New J. Phys.*, Vol. 14, No. 8, 083033, 2012.
24. Miñano, J. C., J. Sánchez-Dehesa, J. C. González, P. Benítez, D. Grabovičkić, J. Carbonell, and H. Ahmadpanahi, "Experimental evidence of super-resolution better than $\lambda/105$ with positive refraction," *New J. Phys.*, Vol. 16, No. 3, 033015, 2014.
25. Born, M. and E. Wolf, *Principles of Optics*, 6th edition, Cambridge University Pres, Cambridge, 1998.
26. Leonhardt, U., S. Sahebdivan, A. Kogan, and T. Tyc, "A simple model explaining super-resolution in absolute optical instruments," *New J. Phys.*, Vol. 17, No. 5, 053007, 2015.
27. Heintzmann, R. and C. Cremer, "Laterally modulated excitation microscopy: Improvement of resolution by using a diffraction grating," *Proc. SPIE*, Vol. 3568, 185–195, 1998.
28. Dunn, R. C., "Near-field scanning optical microscopy," *Chemical Rev.*, Vol. 99, No. 10, 2891–2928, 1999.
29. Lerosey, G., J. De Rosny, A. Tourin, and M. Fink, "Focusing beyond the diffraction limit with far-field time reversal," *Science*, Vol. 315, No. 5815, 1120–1122, 2007.
30. Neice, A., "Methods and limitations of subwavelength imaging," *Advances in Imaging and Electron Physics*, Vol. 163, 117–140, 2010.